ELSEVIER

Contents lists available at ScienceDirect

Biosensors and Bioelectronics

journal homepage: www.elsevier.com/locate/bios





Simultaneous multiparameter whole blood hemostasis assessment using a carbon nanotube-paper composite capacitance sensor

Praveen K. Sekar^a, Xin M. Liang^{b,**}, Seong-Joong Kahng^a, Zhiquan Shu^{a,c}, Anthony B. Dichiara^d, Jae-Hyun Chung^a, Yanyun Wu^{a,***}, Dayong Gao^{a,e,*}

- ^a Department of Mechanical Engineering, University of Washington, Seattle, WA, 98195, USA
- b Wellman Center for Photomedicine, Division of Hematology and Oncology, Division of Endocrinology, Massachusetts General Hospital, VA Boston Healthcare System, Beth Israel Deaconess Medical Center, Harvard Medical School, Boston, MA. 02115. USA
- ^c School of Engineering and Technology, University of Washington Tacoma, Tacoma, WA, 98402, USA
- ^d School of Environmental and Forest Sciences, University of Washington, Seattle, WA, 98195, USA
- ^e Department of Bioengineering, University of Washington, Seattle, WA, 98195, USA

ARTICLE INFO

Keywords: Blood clotting Coagulation function Platelet function Platelet count Hematocrit Smart paper capacitance sensor

ABSTRACT

Rapid and accurate clinical assessment of hemostasis is essential for managing patients who undergo invasive procedures, experience hemorrhages, or receive antithrombotic therapies. Hemostasis encompasses an ensemble of interactions between the cellular and non-cellular blood components, but current devices assess only partial aspects of this complex process. In this work, we describe the development of a new approach to simultaneously evaluate coagulation function, platelet count or function, and hematocrit using a carbon nanotube-paper composite (CPC) capacitance sensor. CPC capacitance response to blood clotting at 1.3 MHz provided three sensing parameters with distinctive sensitivities towards multiple clotting elements. Whole blood-based hemostasis assessments were conducted to demonstrate the potential utility of the developed sensor for various hemostatic conditions, including pathological conditions, such as hemophilia and thrombocytopenia. Results showed good agreements when compared to a conventional thromboelastography. Overall, the presented CPC capacitance sensor is a promising new biomedical device for convenient non-contact whole-blood based comprehensive hemostasis evaluation.

1. Introduction

Hemostasis is a complex physiological cascade in which coagulation factors, platelets and erythrocytes all play prominent roles (Dahlbäck, 2000; Versteeg et al., 2013; Weisel and Litvinov, 2019). Rapid and accurate assessment of these key parameters is imperative in various clinical settings to diagnose, treat, and monitor patients with impaired hemostasis (Jackson, 2011; Mallett and Armstrong, 2015; Tynngård et al., 2015). Over 15 million people worldwide receive oral anticoagulant therapy to prevent and treat life-threatening thromboembolic events, such as deep venous thrombosis, pulmonary embolism, myocardial infarction and stroke (Ageno et al., 2012; Ahrens et al., 2010; Baron et al., 2013; Chen et al., 2020; Kirley et al., 2012; Matchar

Despite their effectiveness in lowering the risk of acute thrombosis, effective anticoagulation management in these patients remains challenging because of the narrow therapeutic window between the increased risk of thromboembolic events from inadequate treatment and the higher probability of dangerous hemorrhage and life-threatening organ failure from over-administration; which is further influenced by numerous food and drug interactions, underlying comorbidities and variability in dose response among patients (Di Minno et al., 2017; Penning-Van Beest et al., 2001; Wells et al., 1994; Zhu et al., 2018). Therefore, patients require frequent laboratory testing of blood clotting

status to ensure appropriate selection of anticoagulant agent and dosing,

which imposes a staggering service load on health care providers

et al., 2000; Pengo et al., 2006; Seiffge et al., 2020; Wang et al., 2020).

[;] CPC, Carbon nanotube-Paper Composite.

^{*} Corresponding author. Department of Mechanical Engineering, University of Washington, Seattle, WA, 98195, USA.

^{**} Corresponding author.

^{***} Corresponding author. Department of Mechanical Engineering, University of Washington, Seattle, WA, 98195, USA. E-mail addresses: xin.m.liang.phd@gmail.com (X.M. Liang), yanyunw@outlook.com (Y. Wu), dayong@uw.edu (D. Gao).

(Matchar et al., 2000; Sullivan et al., 2006). Together, these factors underscore the dire unmet need for inexpensive routine home-monitoring of oral anticoagulation status to advance the quality of care in patients receiving oral anticoagulant therapy and to improve utilization of health care resources.

Traditional laboratory-based clotting assays and devices are not only time-consuming and expensive, but also provide insufficient information due to partial analysis of various individual facetted clotting elements, such as coagulation function (activated partial thromboplastin time - aPTT, prothrombin time - PT, thrombin time - TT), fibrinogen, platelet function (platelet functional analyzer and aggregometry) or blood cellularity (hematology analyzers). Evolving whole blood-based viscoelastic assays such as thromboelastography (TEG) also lack sensitivity and specificity to platelet counts and platelet dysfunction, and can often provide an inaccurate assessment of hemostatic status in the settings of abnormal hematocrit (Bolliger et al., 2012; Ranucci and Baryshnikova, 2020; Spiezia et al., 2008). As a result, each current assay or testing technology has provided an incomplete assessment of bleeding and thrombosis status and risks (Chee and Greaves, 2003; Ganter and Hofer, 2008). This has also stymied the fields of clinical and experimental hematology given the interdependence among the clotting

Over the years, electrical permittivity sensors have been extensively developed to characterize various blood physiological properties that are of relevance for numerous medical applications including hemostasis (Chiba et al., 2015; Hayashi et al., 2008, 2010; Heileman et al., 2013; Pethig, 1984; Ur, 1970). The permittivity change of whole blood in the MHz range was from the accumulation of charge carriers at the interface between erythrocyte membrane and its cytoplasm (Chelidze, 2002), and this was found to change significantly during cellular aggregation, formation of fibrin mesh networks encapsulating the aggregates and retraction of the clot from the contractile force exerted by activated platelets (Asami and Sekine, 2007; Hayashi et al., 2008). So far, two systems that measure blood permittivity using an impedance technique have demonstrated a good sensitivity to both coagulation and platelet function (Hayashi et al., 2015; Maji et al., 2018). One study has reported an independent evaluation of hematocrit level without clotting (Hayashi et al., 2017). These studies confirmed that measuring blood permittivity can provide a sensitive analysis of both cellular and non-cellular blood components that play a key role in hemostasis. However, these impedance-based devices were not able to offer concurrent information on all the key clotting elements from a single assay, and also have limitations in being translated into clinical practice. The physical electrical contact with the blood samples irreversibly contaminates the sensing surface from corrosive elements in the blood (such as proteins and ions). Also, these single-use disposable sensors require precious metal (such as Au or Pt) electrodes to reduce oxidation and electrostatic contamination, in addition to highly specialized impedance analyzers, making them expensive to use in clinical settings. Moreover, the physical electrical contact can also interfere with the natural progression of clotting process in the blood samples. Addressing these challenges in electrical sensor resolution and sensitivity can lead to insights into key components of hemostasis that arise from studying blood permittivity.

In this study, we present a capacitance-based approach for blood permittivity measurement using a carbon nanotube-paper composite (CPC) capacitance sensor fabricated adapting a previously reported techniques (Dichiara et al., 2017; Zhang et al., 2021). A major advancement of the proposed approach is that the capacitance signal obtained from a single measurement could provide three parameters with distinctive sensitivity towards coagulation function, platelet count or function, and hematocrit. The CPC sensor exhibited high fringing field to detect permittivity changes in a blood sample placed in a glass

vial on top of the sensor, eliminating the need for physical electrical contact. The feasibility and sensitivity of this approach was demonstrated using clinically relevant human blood samples. The results were compared against a conventional TEG analyzer to validate the effectiveness of the sensor. To demonstrate potential clinical usefulness, the reduced hemostatic ability, in terms of coagulation function, platelets and hematocrit was evaluated for hemophilia and thrombocytopenia conditions.

2. Material and methods

2.1. CPC capacitance sensor fabrication

Carbon nanotube-paper composite (CPC) film made of multiwall carbon nanotubes (MWCNTs) and cellulose fibers was prepared and fabricated as a capacitance sensor using previously reported techniques (Dichiara et al., 2017; Zhang et al., 2021) (Fig. 1a and b). Briefly, bleached softwood pulp pre-adsorbed with cationic polyacrylamide (CPAM, Percol 3035; BASF, RP, DE) was mixed with a dispersion of sodium dodecyl sulfate (Sigma Aldrich, MO, U.S.A.) and MWCNTs (Cheap Tubes Inc., VT, U.S.A.). The resulting aqueous suspension was subsequently filtered, pressed and dried to form electrically conductive sheets of 60 g m $^{-2}$ containing 10% (w/w)-MWCNTs. The sheets were cut into 5 mm wide strips with 20 mm in length. Silver epoxy (MG Chemicals, BC, CA) was patterned at both the ends to provide electrical contact. The SEM images of CPC surface showed that the cellulose fibers were uniformly coated with the MWCNTs (Supplementary Fig. 1). Controlled water printing and stretching techniques were used to fabricate the CPC capacitance sensors with a V-shaped crack. The V-shaped crack demonstrated a higher sensitivity in comparison to a straight line crack (Zhang et al., 2021) due to larger surface area (approximately 1.4 times). Water was printed on the CPC specimens using a noncontact liquid bridge printing method (Kahng et al., 2018). Then stretching was applied using a tensile test stage to fabricate the sensor electrodes with a gap of 1 mm. The average capacitance for six sensors from the same batch was found to be 314 \pm 12 fF (3.8%; CV). A randomly selected pair of sensors was used for all measurements. Standard cold soldering through copper plates was utilized for external wiring. The fractured CPC was coated with polyurethane and vacuum-sealed on a cover glass (0.17 mm thickness, Thermo Scientific, MA, U.S.A). A polyester film was used to protect the sensor from oxidation and environmental exposure.

2.2. Capacitance measuring system

The experimental setup used for capacitance measurement consists of two CPC capacitance sensors, FDC 2214 capacitance evaluation module (Texas Instruments, TX, U.S.A), glass vials (Agilent Technologies, CA, U.S.A), 3D printed plastic fixtures and styrofoam box, assembled on the orbital shaker (KJ-201 BD, WINCOM, Jiangsu, CHN) as shown in Fig. 1c. FDC 2214 evaluation module was composed of an inductance-capacitance (L-C) circuit to measure capacitance changes as shifts in resonant frequency of the L-C circuit. A 1 nF ceramic capacitor was integrated parallel to the L-C circuit to achieve an excitation frequency of 1.3 MHz (Fig. 1d). A blood sample in glass vials was precisely positioned using plastic fixtures on top of the crack region in the sensor to ensure maximum fringing field for high sensitivity. Fixtures also minimized the variability in sample position between measurements. Bottom fixtures supported the sample weight eliminating any mechanical pressure on the MWCNT-coated cellulose fibers. To reduce the parasitic capacitance, aluminum (Al) foil was used to shield the sensors and the inner surface of the Styrofoam box.

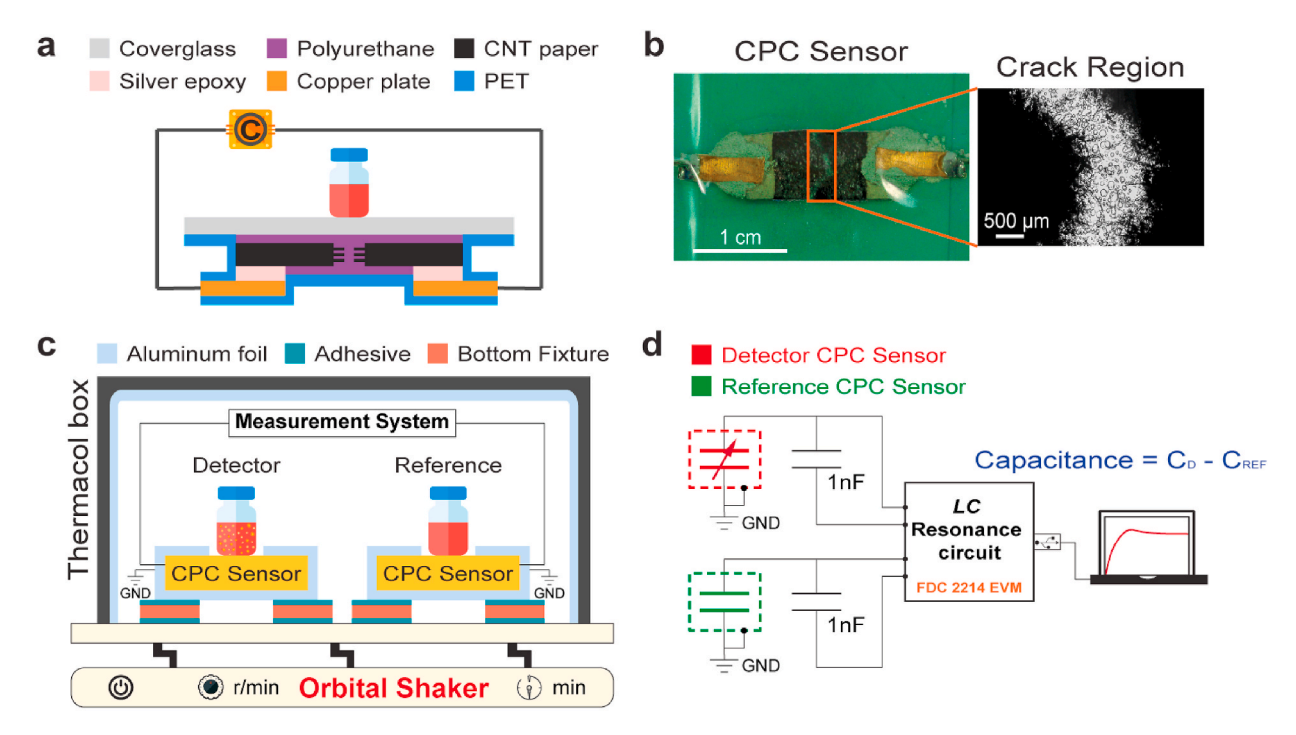


Fig. 1. Capacitance-based hemostasis assessment device. (a) Schematic of the Carbon nanotube-Paper Composite (CPC) capacitance sensor (Not drawn to scale). Human whole blood in glass vial is placed on top of the sensor. The cover glass is supported at the ends through plastic fixtures to avoid stress from sample weight on the carbon nanotube coated cellulose fibers. (b) CPC Sensor: Photograph of a CPC capacitive sensor used in this study. Crack region: Zoom-in view of the crack region (4X), where untangled cellulose fibers formed numerous conductive cantilevers exhibiting high fringing field for capacitance measurements. (c) Schematic layout of the experimental setup and method for hemostasis assessment. (d) Functional block diagram of the measurement system. Laptop with data acquisition and processing software, was used as both power source and data logger.

2.3. Calibration and characterization measurement protocol

Supplementary Fig. 2b illustrates the measurement protocol for sensor calibration and characterization studies (Supplementary Figs. 2c and d.). Briefly, glass vials were placed on top of the sensors and initial capacitance was measured for 5 min. Then, 500 μ L of DI water was added to the reference sensor and allowed to equilibrate for 5 min. Subsequently, 500 μ L of the testing sample was added to the detector sensor and 80-rpm shaking was applied. Measurement was performed for an additional 5 min. Capacitance change from sample addition (8C) was evaluated as the difference between the averaged capacitance before (7–10 min, Supplementary Fig. 2b) and after the addition of testing sample (12–15 min, Supplementary Fig. 2b).

2.4. Clotting measurement protocol

Clotting measurements were conducted using unmodulated blood and blood sample modulated for a predefined platelet count or platelet function or hematocrit, which was generally referred to as blood sample herein. For a CPC-sensor based clotting assay, a baseline capacitance was measured for 5 min with the glass vials placed on the sensors. Then, 325 μL of the blood sample was added to the reference sensor. Immediately, 300 μL of the same blood was added to the detector sensor and 80-rpm orbital shaking was applied. The glass vial on the detector sensor was prefilled with 25 μL of 162.5 mM CaCl $_2$ solution (final Ca $^{2+}$ concentration in whole blood: 12.5 mM) for recalcification of the blood sample. Differential capacitance was measured for an additional 30 min after activation. All measurements were conducted at room temperature (23 °C).

2.5. Analysis of sensing parameters for hemostasis assessments

Capacitance was measured at a sampling rate of 33 Hz during clotting. A real-time average of 300 data points (approximately 9 s) was

performed to obtain a very low frequency envelop for capacitance change with the progression of clotting. For data analysis and presentation (graphs), the initial time (t=0) was defined as the time point when the blood sample was activated. T_{Cpeak} was the timepoint for maximum capacitance value after activation. $\Delta C1$ was evaluated as the magnitude decrease in capacitance from peak to a steady state value. Steady state capacitance was the averaged value between 28 and 30 min after activation. $\Delta C2$ was the maximum capacitance value after activation.

2.6. Blood samples

Fresh whole blood in standard 3.2% citrate tubes were purchased from Bloodworks Northwest Seattle, WA. Unless specified, all blood samples were from de-identified, healthy volunteers without previously known coagulation or platelet disorders, and had not received any antithrombotic medication in the two weeks prior to sample collection. Blood tubes were transported and stored in a styrofoam box at room temperature and used within 4 h from blood draw. CaCl2 solution in phosphate buffered saline (PBS, pH 7.4; Sigma-Aldrich, MO, U.S.A) was prepared on the day of experiments. In some experiments the blood samples were treated in vitro to modulate platelet count or platelet function or hematocrit to systematically study their effects on the sensing parameters (T_{Cpeak} , $\Delta C1$ and $\Delta C2$). Blood samples with a predefined platelet count or hematocrit were prepared from two-step centrifugation technique. First, citrated whole blood was centrifuged at 200 g for 10 min to pellet down the erythrocytes. Desired volume of the resultant supernatant, platelet-rich-plasma (PRP) was carefully removed. Subsequently, a part of the collected PRP was further centrifuged at 4000 g for 5 min to obtain platelet-poor-plasma (PPP). The erythrocyte pellet was then resuspended in the remaining PRP by gently inverting the tube to get a reconstituted hematocrit modulated sample. The reconstituted sample was then divided into portions and diluted with calculated volume of PRP and PPP to yield a blood sample with a

predefined hematocrit (15, 20, 40 and 50%) or platelet count (100, 120, 140, 160 and 180×10^3 platelets μl^{-1}).

Platelet counts in all hematocrit modulated samples were maintained constant as $165 \pm 27 \times 10^3$ platelets μl^{-1} . Similarly, the hematocrit of all platelet count modulated samples was 40 \pm 3%. Platelet functional inhibition was done by incubating the samples with a predefined concentration of aspirin (0, 0.1, 0.51 mM). Aspirin (Sigma-Aldrich, MO, U.S.A) was dissolved in dimethyl sulfoxide (DMSO; Sigma-Aldrich, MO, U.S.A) and diluted with PBS to a desired concentration before adding to blood samples. In the aspirin study, appropriate amount of PBS buffer was added to the control samples to maintain approximal cell counts and hemodilution as the aspirin-treated samples. Platelet counts and hematocrit in whole blood, PRP and PPP were measured using a hematology analyzer (XP-300, Sysmex America OR, U.S.A) with an accuracy of 1.5% for hematocrit and $\pm 6 \times 10^3$ μl^{-1} for platelet counts. In general, ethylenediaminetetraacetic acid (EDTA) is preferred for blood cellularity measurements to avoid hemodilution (Briggs, 2009). However, EDTA irreversibly chelates the free calcium in blood and permanently affects the progression of coagulation cascade and the ability of the blood cells to form aggregates and deform from retraction forces (Green et al., 2008). Therefore, blood counts were measured on blood samples anticoagulated with sodium citrate and reported with 10% hemodilution.

2.7. Thromboelastography (TEG)

TEG measurements were performed by trained personnel at the Department of Laboratory Medicine, University of Washington using TEG 5000 thromboelastograph hemostasis analyzer (Haemonetics, U.S. A). *R-time* parameter is the time from the start of the measurement to the initial detection of clot formation (in min) and is indicative of the coagulation function. MA is a measure of clot strength as determined by the ability of platelets to bind via $\alpha_{\text{IIb}}\beta_3$ integrin as well as the elasticity of the fibrin mesh (Gottumukkala et al., 1999). The newly introduced sensing parameters, T_{Cpeak} and $\Delta C1$, were compared with the equivalent TEG diagnostics parameters R-time and MA, respectively. TEG measurements were performed within 5 h from blood draw. Blood samples were activated with 12.5 mM CaCl₂ (Citrated Native TEG), similar to measurements using the CPC capacitance sensor.

2.8. Statistical analysis of data

To ensure excellent data repeatability and reliability, the sample size for the sensing parameters characterization study was predetermined to be five healthy donors to account for biological variability with two replicate measurements each. For TEG comparison study, blood samples from twelve healthy donors with single replicate measurement was used. Three hemophilia patient samples and simulated thrombocytopenia samples were used to investigate the potential clinical applications for the sensor. Platelet count and hematocrit of blood samples were obtained as an average of three measurements using a hematology analyzer. The vast majority of the data distributions were found to be normal (Shapiro-Wilk Goodness of Fit for normal distribution, p > 0.077) and were analyzed using parametric methods for statistical analysis. For the two measurements that contained distributions significantly skewed from normal (Fig. 5f, Supplementary Fig. 6b), nonparametric methods were used for statistical analysis. Pearson's correlation coefficient (r) was used to evaluate linearity between the pairs of data. One-way analysis of variance (ANOVA) with Tukey's post-hoc or Kruskal-Wallis tests was used to compare the results with three or more groups. Two-sided unpaired t-test was used for comparison between healthy donors and hemophilia patients. Two-sided paired t-test or Wilcoxon matched-pairs signed rank test was used to compare between healthy and thrombocytopenia samples. * denotes a p-value less than 0.05 and was considered statistically significant. ** denotes a p-value less than 0.01 and NS denotes not significant.

3. Results

3.1. Characterization of the capacitance-based hemostasis assessment

A blood sample was placed on a carbon nanotube-paper composite (CPC) capacitance sensor made of multiwall carbon nanotubes (MWCNTs) and cellulose fibers (Fig. 1a and b). The CPC sensor contained a fractured region where MWCNTs-coated cellulose fibers formed numerous conductive cantilevers (Fig. 1b - Crack region, 4X) exhibiting a high fringing field for capacitance measurement. A differential measurement using two CPC capacitance sensors was chosen to minimize the environmental disturbances (Fig. 1c and d). This design provided a capacitance signal with low noise in the order of 200 aF (peak-to-peak; Supplementary Fig. 2a). Calibration experiment using reference liquid samples showed that a linear relationship exists between the capacitance change (δC) and the permittivity the references (r = 0.99, p <0.00001, n = 7; Pearson's correlation; Supplementary Fig. 2c). Additional measurements using NaCl solutions confirmed that δC sensitively followed the permittivity decrease from increasing molar concentration of *NaCl* in DI water (F(2.02, 8.07) = 414.4, p < 0.00001, n = 11; ANOVA;Supplementary Fig. 2d).

To minimize the differential capacitance variation due to rouleau formation and cell sedimentation, blood samples were gently agitated on an orbital shaker (Fig. 1c). In practice, 80-rpm orbital shaking was applied, since this speed sufficiently minimized cell sedimentation from rouleau formation (Supplementary Fig. 3a) and provided a stable reference capacitance (80-rpm cycle, Supplementary Fig. 3b). Capacitance measurement at various operating frequency (120k, 550k, 1.3M, 3.1M, and 5.3M Hz), using blood samples with a predefined hematocrit (0, 10, 20, 30%), showed that δC at 1.3 MHz was by approximately 125% higher than at 120 kHz for 30% hematocrit (Fig. 2). This finding suggests that the frequency-dependent permittivity response of blood was pronounced at 1.3 MHz, similar to previous studies (Abdalla, 2011; Maji et al., 2017). At this frequency, δC also linearly increased with higher hematocrit (r = 0.92, p < 0.001, n = 3; Pearson's correlation).

When testing a blood sample with $CaCl_2$ (final concentration: 12.5 mM), we observed that capacitance increased and reached a peak value before decreasing to a steady state value (Fig. 3a). To ensure that the signal was from clotting, the same blood sample was tested without

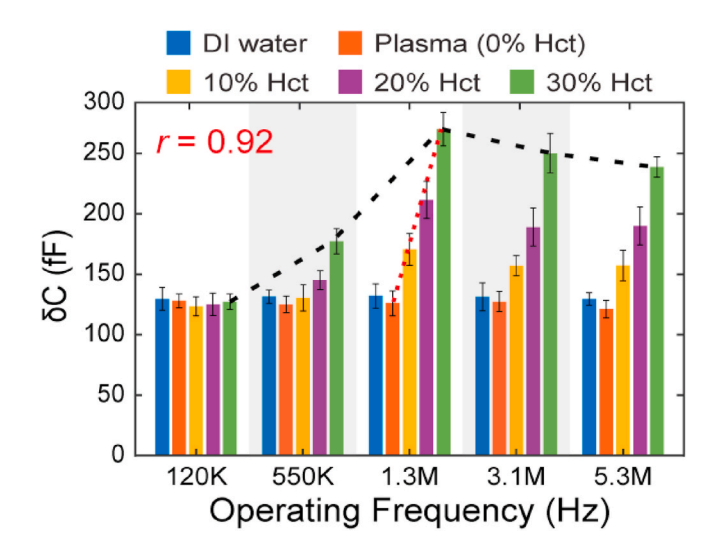


Fig. 2. Capacitance change with sample addition (δC) for various operating frequency. Peak δC was observed at 1.3 MHz for all hematocrits; n=3 with single replicates; Bars represent mean values; error bar, S.D. At 1.3 MHz, δC linearly increases with hematocrit; *Pearson's* r=0.92. (For interpretation of the references to colour in this figure legend, the reader is referred to the Web version of this article.)

recalcification following the same procedure. Capacitance was stable for the inactivated sample with a *peak-to-peak* change of 414 aF (Supplementary Fig. 4a), which confirmed that the capacitance signals in Fig. 3a was caused by clotting. The capacitance trend during clotting was similar to the permittivity changes that have been observed in previous impedance systems (Hayashi et al., 2015; Maji et al., 2018). Clotting was not observed in the inactivated sample, which indicated that shaking did not generate a non-physiologically high shear environment to activate the platelets (photographs in Supplementary Fig. 4a). Moreover, the shaking also did not interfere with the natural progression of clotting for activated blood sample (Supplementary Fig. 4b).

3.2. A multiparameter assessment of hemostasis: simultaneous assessment of coagulation time, platelet count or function, and hematocrit

To examine the ability of our sensor to simultaneously assess coagulation function, platelets and hematocrit, the blood samples from healthy donors were modulated for a predefined clotting activation level (Ca^{2+} concentration), platelet count or function, or hematocrit. From the measured capacitance, three parameters namely T_{Cpeak} , $\Delta C1$ and $\Delta C2$ (Fig. 3a) were chosen for analysis. We found that T_{Cpeak} decreased with increasing CaCl_2 concentration (6.3, 12.5 and 25 mM; Fig. 3b), which indicated a trend in T_{Cpeak} and coagulation time (F(2,27)=27.16, p<

0.00001; ANOVA). For the remaining studies, 12.5 mM CaCl₂ was used to activate clotting in the samples. When we tested blood samples with a predefined platelet count (100, 120, 140, 160 and 180×10^3 platelets μl^{-1}), we found that $\Delta C1$ linearly increased with increasing platelet count (r = 0.94, p < 0.00001; Pearson's correlation; Fig. 3c). From measurements using blood samples incubated with aspirin (0, 0.1, 0.51 mM), which inhibits platelet activation, we found that $\Delta C1$ dosedependently decreased with increasing aspirin concentrations (F (2,27) = 17.68, p < 0.0001; ANOVA; Fig. 3d). Together, the above two results (Fig. 3c and d) showed that $\Delta C1$ was sensitive to both platelet count and function. When we tested blood samples with a predefined hematocrit (15, 20, 40 and 50%), we found that $\Delta C2$ linearly increased with increasing hematocrit (r = 0.96, p < 0.00001; Pearson's correlation; Fig. 3e). Collectively, the above results showed that the sensor can offer a multiparameter assessment of hemostasis by providing concurrent information on coagulation function, platelet count or function, and

Additionally, the sensing parameters, T_{Cpeak} , $\Delta C1$, and $\Delta C2$, showed distinctive sensitivities towards coagulation function, platelet count or function and hematocrit, respectively. T_{Cpeak} did not change significantly with platelet count (r=0.18, p=0.17; Pearson's correlation; Supplementary Fig. 5a), aspirin concentration (F(2,27)=0.082, p=0.92; ANOVA; Supplementary Fig. 5b), and hematocrit (r=0.08, r=0.92).

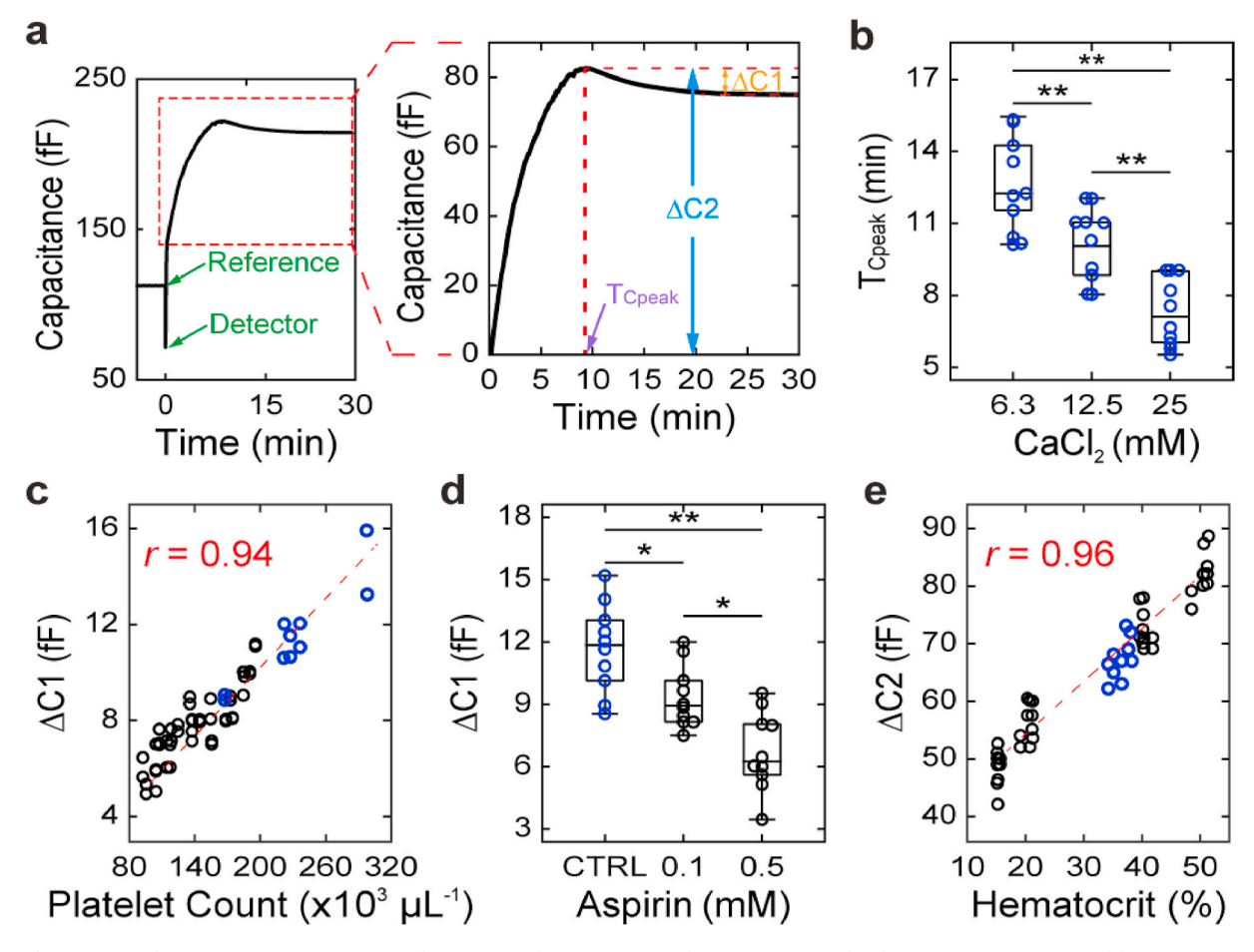


Fig. 3. Multiparameter hemostasis assessment: Simultaneous evaluation of coagulation function, platelet count or function and hematocrit. (a) Left: A representative overall capacitance signal for a blood sample activated using CaCl₂ (12.5 mM). **Right:** Zoom-in view of the region of interest with the sensing parameters, T_{Cpeak} , Δ C1, and Δ C2 for analyses. (b) T_{Cpeak} decreases with increasing concentration of activating CaCl₂ (mM). (c) Δ C1 linearly increases with platelet count in the range 93–298 × 10³ platelets μ l⁻¹; *Pearson's r* = 0.94. (d) Δ C1 decreases dose-dependently with aspirin treatment. (e) Δ C2 linearly increases with hematocrit in the range 15.1%–51.2%; *Pearson's r* = 0.96. For (b - e): n = 5 healthy donors with two replicate measurements. Black circles are results from blood samples treated *in vitro* to modulate platelet count or platelet function or hematocrit, and blue circles are results from blood samples without any such treatments. All box plots with whiskers represent data distribution (Maximum, Third quartile, Median, First quartile, Minimum). p-values were calculated from one way ANOVA with Tukey's post-hoc. *p < 0.05 and **p < 0.01. (For interpretation of the references to colour in this figure legend, the reader is referred to the Web version of this article.)

0.57; Pearson's correlation; Supplementary Fig. 5c). $\Delta C1$ did not show a statistically significant difference with CaCl₂ concentration (F(2,27)=0.14, p=0.87; ANOVA; Supplementary Fig. 5d) and hematocrit (r=0.037, p=0.80, Pearson's correlation; Supplementary Fig. 5e). We observed that $\Delta C1$ was higher for unmodulated blood samples compared to blood samples modulated to a predefined hematocrit (p<0.0001; Paired t) due to variations in platelet count between the two groups (Blue circles: 249 ± 37 , Black circles: 165 ± 27 , x 10^3 platelets μ 1-1). This finding was consistent with our result in Fig. 3c, suggesting platelet count to be a major factor affecting $\Delta C1$. $\Delta C2$ had a positive correlation only with hematocrit and no statistically significant changes was detected with variations in CaCl₂ concentration (F(2,27)=0.064, p=0.94; ANOVA; Supplementary Fig. 5f), platelet count (r=-0.19, p=0.15; Pearson's correlation; Supplementary Fig. 5g) and aspirin concentration (F(2,27)=0.23, p=0.8, ANOVA; Supplementary Fig. 5h).

To evaluate the stability of our system, repeated measurements were conducted using room temperature stored blood samples with predefined storage durations (45, 90, 180, 270 and 330 min) after blood draw. We observed a significant decrease in T_{Cpeak} for blood samples stored for 270 and 330 min, relative to measurements at 45 min (F(4,20)) = 6.72, p < 0.045; ANOVA Tukev's post-hoc, Supplementary Fig. 6a). No significant difference was observed for blood samples tested at 90 and 180 min compared with 45 min ($p \ge 0.96$; ANOVA Tukey's posthoc). No significant difference was observed in $\Delta C1$ (H(4) = 0.89, p =0.93; Kruskal-Wallis test; Supplementary Fig. 6b) and $\Delta C2$ (F(4,20) =0.28, p = 0.89; ANOVA; Supplementary Fig. 6c) for all groups. These results have shown good repeatability in the newly introduced sensing parameters for in vitro evaluation of hemostasis using citrated blood. Furthermore, all sensing parameters, T_{Cpeak} , $\Delta C1$, and $\Delta C2$, demonstrated a gaussian distribution trend for the healthy volunteers tested, as shown in Supplementary Fig. 7 ($p \ge 0.16$, n = 26; Shapiro-Wilk test).

3.3. Comparison with thromboelastography (TEG)

To evaluate the potential clinical utility of our sensor, we compared the coagulation time and platelet parameters with the clinically relevant diagnostic parameters of citrate native thromboelastography (CN-TEG) assay. Results illustrated a strong positive correlation between T_{Cpeak} and Reaction time (R-time) (r=0.95, p<0.00001, n=12; Pearson's correlation, Fig. 4a). The obtained data validated the effectiveness of the presented sensor in evaluating coagulation function and is in good agreement with the viscoelastic TEG assay. However, there was a relatively less degree of correlation between $\Delta C1$ and Maximum Amplitude (MA) (r=0.58, p=0.050, n=12; Pearson's correlation, Fig. 4b). The reason for such discrepancy is likely because the MA parameter, which measures clot strength, may be affected by both the number of cells in the clot and passive fibrin elasticity (Gottumukkala et al., 1999). To

examine the hypothesis, we rearranged the data as illustrated in Fig. 4c. Interestingly, a much stronger correlation between $\Delta C1$ and platelet count than to *MA* was observed ($\Delta C1: r = 0.91, p < 0.0001; MA: r = 0.62,$ p = 0.033; Pearson's correlation), suggesting $\Delta C1$ may be solely dependent on the platelet count. This also implies that $\Delta C1$ might be a better alternative in evaluating platelet count-related diseases as it may have a higher sensitivity and specificity to platelet count. Furthermore, the common clinical practice to assess the individual contribution of fibrin(ogen) and platelets to MA, is to use a modified TEG assay, where an $\alpha_{IIb}\beta_3$ antagonist is introduced to ensure all viscoelastic parameters measured are the result of fibrin formation alone (Gottumukkala et al., 1999; Whiting and DiNardo, 2014). Our results suggests that the proposed sensor could potentially eliminate the need of using additional specialized inhibitors to assay platelets in whole blood, which could further minimize the chances of pre-analytical errors that complicate existing assays (Adcock Funk et al., 2012).

3.4. Evaluation of clotting function in hemophilia patients and simulated thrombocytopenia condition

To examine the potential usefulness of our sensor in the context of hematologically altered conditions, we conducted measurements using blood samples with clotting disorders. To investigate the clinical relevance in the context of a coagulation disorder, we tested blood samples from three hemophilia patients (2 Hemophilia A, 1 Hemophilia B). The absence of functional factor VIII or factor IX resulted in a significantly higher T_{Cpeak} relative to healthy samples (t = 8.47, df = 5.5, p < 0.001; Unpaired t; Fig. 5a). This finding showed that T_{Cpeak} was sensitive to coagulation factor deficiency and can potentially be used to monitor coagulation function in hemophilia patients. We noted that the platelet count and hematocrit were in the normal or close to normal ranges for the hemophilia patient samples (Platelet count: 184 ± 37 platelets μl^{-1} , Hematocrit: 35.8 \pm 2.77%; n = 3). We found no significant differences in both $\Delta C1$ (t = 1.11, df = 5.56, p = 0.31; Unpaired t; Fig. 5b) and $\Delta C2$ (t =0.66, df = 5.85, p = 0.54; Unpaired t; Fig. 5c) for hemophilia patients compared to healthy individuals. These results suggested that platelet function or count, and hematocrit were not significantly impacted by a coagulation factor deficiency in these patient samples.

To demonstrate the clinical relevance in the context of a quantitative platelet disorder, platelet counts in healthy blood samples were modulated to be less than 50×10^3 platelets μl^{-1} to induce a thrombocytopenia condition. Interestingly, we observed a statistically significant increase in T_{Cpeak} for blood samples with a very low platelet count compared to healthy samples (t=3.23, df=5, p=0.023; Paired t; Fig. 5d). This was in contrast to our previous result, where T_{Cpeak} demonstrated characteristic sensitivity to coagulation function by showing no significant difference with variations in platelet count in the

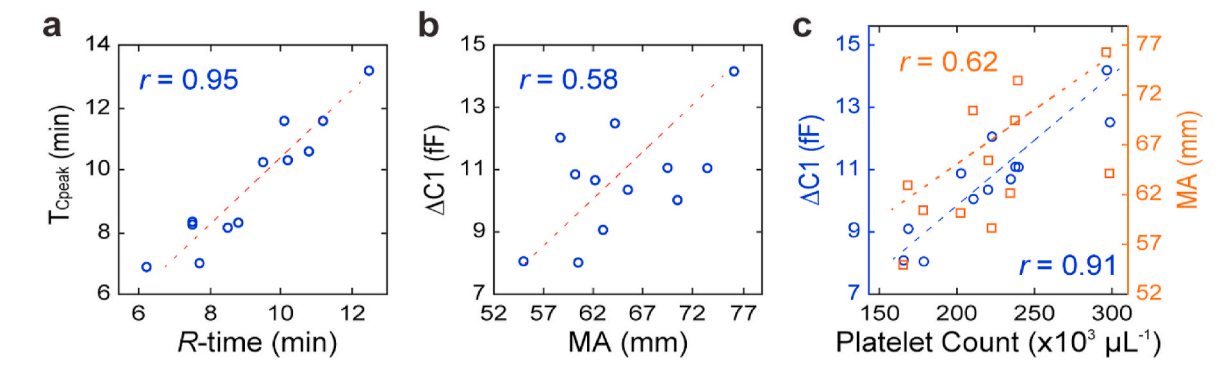


Fig. 4. Comparison with Thromboelastography (TEG). (a) T_{Cpeak} shows a strong positive correlation with the Reaction time (*R*-time) parameter demonstrating a good agreement with TEG in evaluating coagulation function; *Pearson's* r=0.95 (b) Less degree of correlation between ΔC1 and Maximum Amplitude (*MA*) parameter of TEG; *Pearson's* r=0.58. (c) ΔC1 shows a stronger positive correlation with platelet count in comparison to MA; *Pearson's* r-MA: r=0.62, ΔC1: r=0.91. For all graphs: n=12 healthy donors with single replicate measurement using the presented CPC capacitance sensor and concurrent Citrate Native TEG.

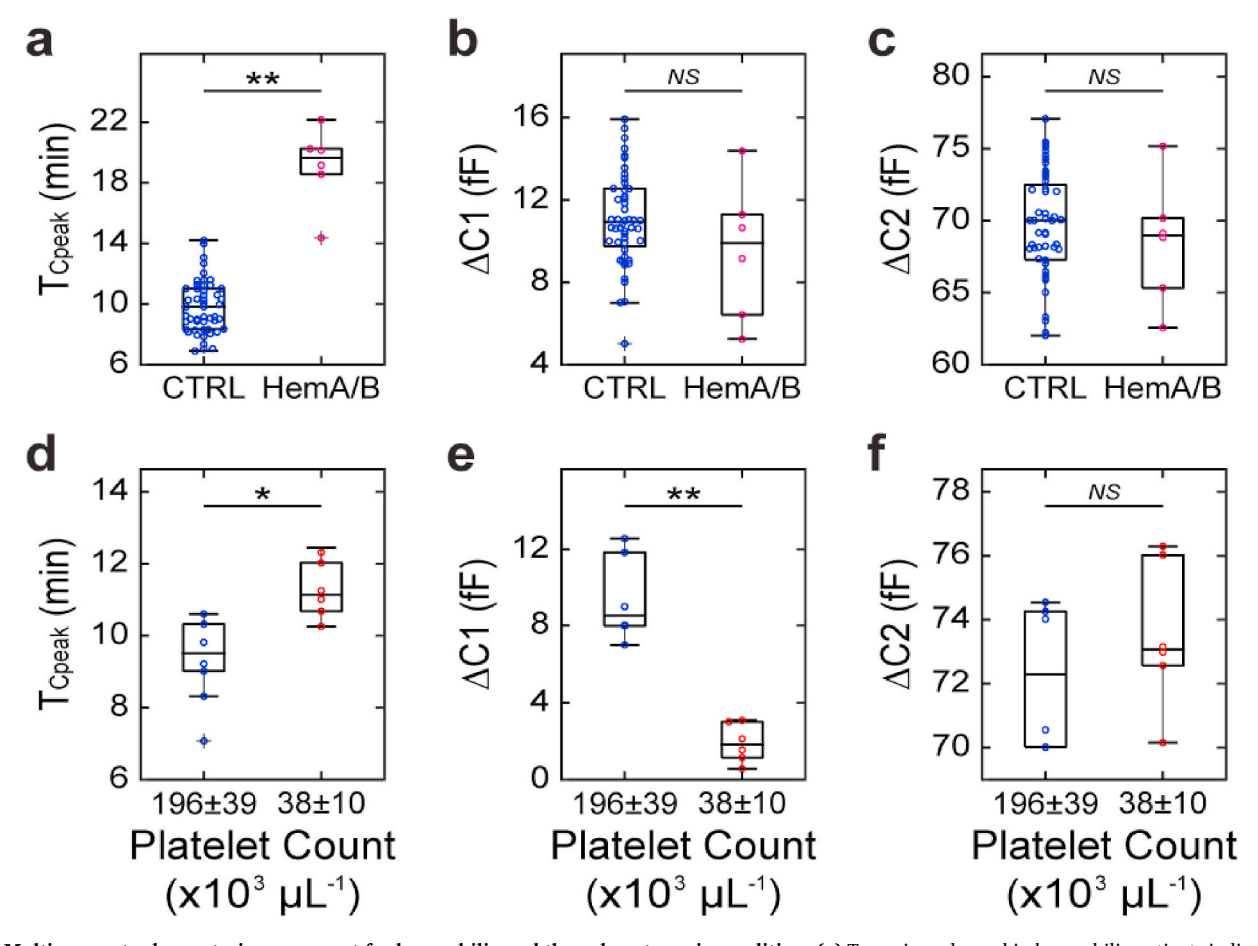


Fig. 5. Multiparameter hemostasis assessment for hemophilia and thrombocytopenia condition. (a) T_{Cpeak} is prolonged in hemophilia patients indicating the presence of coagulation factor deficiency. (b) Δ C1 and (c) Δ C2 showed no significant difference between healthy and hemophilia patients. (d) T_{Cpeak} is prolonged for blood samples with a thrombocytopenia condition. (e) Δ C1 is significantly reduced from a severe quantitative platelet depletion. (f) Δ C2 showed no significant difference between healthy and severe thrombocytopenia conditions. For (a, b, c): n = 26 healthy donors and n = 3 hemophilia patients (2 hemophilia A, 1 hemophilia B) with 2 replicate measurements. p-values were calculated from two-sided unpaired p-test. For (d, e, f): p-3 healthy and thrombocytopenia samples with 2 replicate measurements. For (d, e): p-values were calculated from two-sided paired p-test. For (f): p-value was calculated from Wilcoxon matched-pairs signed rank test. p-4 0.05, p-4 0.01 and NS denotes not significant. All box plots with whiskers represent data distribution (Maximum, Third quartile, Median, First quartile, Minimum, with outliers beyond).

range of 93–298 \times 10³ platelets μ l⁻¹ (Supplementary Fig. 5a). The reduced T_{Cpeak} observed in blood samples with platelet count less than 50×10^3 platelets μl^{-1} is indicative of the multifaceted role played by platelets in hemostasis. In addition to their key role in primary hemostasis, platelets also play an active role in secondary hemostasis (coagulation cascade) by providing binding sites for coagulation factors in thrombin generation (van der Meijden and Heemskerk, 2019; Michelson, 2019). Therefore, it is possible that a lower activated platelet population could diminish the interaction and localization of the coagulation factors, which further slows down the thrombin generation. As expected, we observed a significant decrease in $\Delta C1$ compared to healthy samples (t = 8.79, df = 5, p < 0.001; Paired t; Fig. 5e), reaffirming the sensitivity of $\Delta C1$ to platelet counts. Since hematocrit of thrombocytopenia samples was close to healthy samples (Thrombocytopenia: 40.7 \pm 2.9%; Healthy: 38.1 \pm 2.1, n=3), no statistically significant difference was observed in $\Delta C2$ (W = 9, p = 0.44; Wilcoxon matched-pairs signed rank test; Fig. 5f).

Taken together, these studies demonstrated the potential usefulness of our sensor and highlight the advantages of a simultaneous assessment of cellular and non-cellular components of hemostasis. Furthermore, these preliminary results suggest that the sensor can be used to study the synergistic relationship between coagulation factors, platelets and erythrocytes in the hemostatic process for normal and different disease states.

4. Discussion

Motivated by the importance of having a rapid, accurate and convenient hemostasis assessment device, we have developed the first reported capacitance-based approach with a unique ability to multiplex the assessment of coagulation function, platelets and hematocrit in a single measurement. The CPC capacitance sensor described here provides several attractive advantages over existing clinical assays and devices as summarized in Table 1. Its ease of use without the necessity of extensive sample preparation or to be performed only by a highly trained laboratory personnel, and additional benefits, such as noncontact measurement, high reusability and low cost, makes it an ideal tool to readily evaluate clotting status while significantly reducing the financial burden on primary care resources. It may also be used for therapeutic monitoring of anticoagulants, antiplatelet agents, and factor replacement.

The principle of blood permittivity variation during clotting has been described previously (Hayashi et al., 2010). Earlier attempts using impedance-based sensors have demonstrated the clinical utility by differentiating limited aspects of coagulation and platelet function between normal and pathophysiologic states (Hayashi et al., 2015; Maji et al., 2017). However, the presented capacitance-based approach also offers a simultaneous hematocrit assessment not found in any existing clinical devices including the previous impedance-based sensors.

Table 1Potential advantages of the presented CPC capacitance sensor over currently available alternate approaches.

Features	Presented CPC capacitance Sensor	Viscoelastic Assays	Traditional laboratory assays	Blood gas or hand- held analyzers
Provide global assessment of hemostasis and evaluate bleeding risk in a single device	1			
Provide global assessment of hemostatic status (coagulation time + platelet function)	/	/		
Can measure platelet count	✓		✓	
Can measure hematocrit	✓		✓	1
Rapid Turnround Time (TAT): No need for blood sample	1	1		/
processing Ease of use: No need for trained	1			1
laboratory staff Cost efficient: Reusability	✓			1

Simultaneous assessment of clotting function and hematocrit can facilitate the development of automated alert or correction algorithm for blood samples with elevated hematocrit (>60%) and eliminate the need for in vitro citrate adjustment (Marlar et al., 2006). Fibrinogen (Factor I), a key clotting parameter converted to fibrin by thrombin during coagulation, plays a key role in the rapid encapsulation of blood cells and in the propagation of platelet contractile forces through the mesh network for clot retraction (Michelson, 2019; Sørensen et al., 2011; Versteeg et al., 2013). Reduced and/or dysfunctional fibrinogen can lead to pathological bleeding (Kattula et al., 2017). In addition, various blood physiological parameters such as blood types, concentration of ions (such as Na+, Ca2+ and K+), proteins (such as albumin) and vitamins (such as Vitamin K) may have an impact on blood hemostatic ability and could also influence the inferences from clotting assays (Chakraverty et al., 1996; Gissel et al., 2016; Mann, 1999; Rasmussen et al., 2016). It remains to be seen whether the CPC capacitance sensor could offer reliable hemostatic assessments with the presence of these biological variabilities.

Another unique feature of the sensor is the ability to provide diagnostic parameters with distinctive sensitivity to coagulation function, platelet count or function, and hematocrit. Specifically, in our system the coagulation and platelet function assessments were not interfered by variations in hematocrit (Supplementary Figs. 5c and e). This was in contrast to viscoelastic whole blood assays, which can provide inaccurate assessments for abnormal hematocrit settings (Nagler et al., 2013; Ogawa et al., 2012). AC2 provided an exclusive assessment of hematocrit by not changing significantly with variations in clotting activation levels, platelet count and platelet function (Supplementary Figs. 5f-h). The blood permittivity response at 1.3 MHz was from the accumulation of charge carriers at the interface between the erythrocyte membrane and its cytoplasm (Chelidze, 2002). Our experimental results suggest that the magnitude of capacitance change (∞ permittivity change) due to redistribution of these accumulated charge carriers from cellular aggregation and encapsulation of the aggregate structures in a fibrin mesh during the clot growth phase, was dependent on the erythrocyte

concentration in whole blood.

Our results suggests that the presented sensor affords a simple approach for studying the synergistic relationship between cellular and non-cellular components of hemostasis in normal and different disease states. For example, platelet function in hemophilia patients has been debated and few studies have reported various alterations, such as increased platelet P-selectin expression, lower aggregation upon coincubation with tissue factor, or reduced platelet contractile forces during clot formation in comparison to healthy individuals (van Bladel et al., 2011; Grünewald et al., 2002; Jensen et al., 2013). However, these conclusions were from assays on platelet suspensions or platelet-rich plasma which only partially reflect platelet function in hemostasis in vivo (Harrison, 2009). In our study, results from a limited number of hemophilia patients suggested that platelet function was not significantly impacted by hemophilia conditions (Fig. 5b). Data obtained from a small number of thrombocytopenia samples revealed a prolonged T_{Cpeak} (i.e., coagulation time) (Fig. 5d). Similar observations have been made from previous assays (Baughman et al., 1993; Chakraverty et al., 1996; Levi and Opal, 2006). However, these existing assays cannot interpret such prolongation in coagulation time as arising from a severe platelet depletion without an independent platelet count measurement. In our device, in addition to a prolonged T_{Cpeak} , we also observed a significant decrease in $\Delta C1$, as it primarily depends on platelet count, therefore the prolongation in coagulation time may be better deciphered as originating from the reduced platelet count. Additionally, it is also possible to integrate an array of CPC capacitance sensors to conduct parallel assays to analyze blood samples with complex or multiple clotting disorders. These highlight the research-enabling aspect of our technology and the ability to test or create new hypotheses. In a clinical setting, parallel clotting assays could potentially expedite the assessment of bleeding risks in patients, who are not easily diagnosed from a single assay.

Unfortunately, like all other in vitro devices, the presented device does have certain limitations. Firstly, after activation, sedimentation of microthrombi over time due to growing size of the aggregates (Supplementary Fig. 4b) may convolute the measurement. In the developed system, the sedimentation occurs perpendicular to the electrode plane, hence it's likely to have contributed to capacitance increase during the initial stage of clotting (Asami and Hanai, 1992). The possibility of adding additional sensors in a plane parallel to the sedimentation direction to minimize the signal artifacts from sedimentation will be explored in our future work. Two identical CPC capacitance sensors fabricated from a single batch were reused for all measurements in this study. It is possible that there might be some small differences in the intrinsic capacitance value and sensitivity between the sensors due to variations in MWCNTs dispersion and composite fracture. However, by conducting a single point calibration study using the pair of sensors one could establish the sensitivity of the system.

To circumvent the reference signal changes due to rouleau formation and subsequent sedimentation, the system requires constant mechanical vibration/shaking, which limits the realization as a handheld analyzer like CoaguChek (Roche Diagnostics), Xprecia Stride (Siemens Healthineers), or i-STAT (Abbott). While these handheld analyzers may offer a more convenient way to extract physiological properties of blood at bedside, they have shown to exhibit variable performance and are limited to specific applications like monitoring patients on warfarin therapy (Harris et al., 2013). Furthermore, they don't provide information on platelet function or count, resulting in a crude snapshot of the hemostatic status. Majority of the clotting assays are still limited to sophisticated laboratories with well-trained operators and personnel for interpreting the results (Harris et al., 2013). The long delay associated with these assays limits their use in acute care settings or patient with active bleeding (Gillissen et al., 2018). In comparison, our system can easily be realized as an automated device with minimal human interventions because of no need for sample processing, limited disposables and minimal steps involved for a clotting measurement. In our future work, we plan to develop an automated compact self-contained bench-top version of the presented system. The system components including the orbital shaker can be customized to compact sizes using rapid prototyping techniques. Additionally, the instrumentation for capacitance sensor can also be miniaturized on custom-made circuit board.

5. Conclusion

In this study, we reported the first non-contact capacitance-based hemostasis assessment using a novel carbon nanotube-paper composite (CPC) sensor. CPC capacitance measurements at 1.3 MHz provided three sensing parameters, namely T_{Cpeak} , $\Delta C1$ and $\Delta C2$, to independently assess coagulation function, platelet function or count, and hematocrit respectively. The presented sensor was characterized using reference permittivity liquids and then applied to evaluate the hemostatic ability of blood samples with varying clotting activation levels, quantitative and qualitative platelet defects, and different hematocrits. The testing results showed good agreements with a conventional TEG analyzer. Potential clinical usefulness of the sensor was demonstrated by testing hemophilia patient samples and blood samples simulated with thrombocytopenia condition. Finally, the presented CPC capacitance sensor is a promising new diagnostic device for convenient comprehensive evaluation of hemostasis with attractive advantages such as whole-blood based non-contact evaluation of multiple key clotting biomarkers with high accuracy, high sensitivity and low cost. In our upcoming study, we will explore the ability of the CPC sensor to analyze disorders arising from various pathological conditions. Future work will also be on developing an automated compact self-contained bench-top version of the presented system.

CRediT authorship contribution statement

Praveen K. Sekar: Conceptualization, Methodology, Software, Investigation, Formal analysis, Data curation, Writing, Visualization, Funding acquisition. Xin M. Liang: Conceptualization, Methodology, Formal analysis, Data curation, Validation, Resources, Writing, Visualization, Supervision, Project administration. Seong-Joong Kahng: Methodology, Sensor fabrication. Zhiquan Shu: Methodology, Validation. Anthony B. Dichiara: Methodology, Composite fabrication. Jae-Hyun Chung: Conceptualization, Methodology, Formal analysis, Validation, Resources, Writing, Supervision, Project administration, Funding acquisition. Yanyun Wu: Conceptualization, Methodology, Formal analysis, Data curation, Validation, Resources, Writing, Visualization, Supervision, Project administration, Funding acquisition. Dayong Gao: Conceptualization, Methodology, Formal analysis, Data curation, Validation, Resources, Writing, Visualization, Supervision, Project administration, Funding acquisition. Project administration, Funding acquisition.

Declaration of competing interest

The authors declare the following financial interests/personal relationships which may be considered as potential competing interests: A U.S provisional patent application has been filed covering the capacitance based hemostasis assessment approach ("Patent Applied For")

Acknowledgements

The authors thank Dr. Ren Shen, Dr. Jason Acker and Mr. Vigneshwar Sakthivelpathi for helpful discussion and technical assistance. This work was supported by the generous gifts from the CoMotion Innovation Fund at University of Washington (682548, D.Y.G.) and Advanced Manufacturing Program of National Science Foundation grant (1927623, J.C.). The authors also thank the Biology Imaging Facility at the University of Washington and the Harvard Center for Biological Imaging for infrastructure and support.

Appendix A. Supplementary data

Supplementary data to this article can be found online at https://doi.org/10.1016/j.bios.2021.113786.

References

Abdalla, S., 2011. AIP Adv. 1, 012104.

Adcock Funk, D.M., Lippi, G., Favaloro, E.J., 2012. Semin. Thromb. Hemost. 38, 576–585.

Ageno, W., Gallus, A.S., Wittkowsky, A., Crowther, M., Hylek, E.M., Palareti, G., 2012. Chest 141, e445–e885.

Ahrens, I., Lip, G.Y.H., Peter, K., 2010. Thromb. Haemostasis 104, 49-60.

Asami, K., Hanai, T., 1992. Colloid Polym. Sci. 270, 78-84.

Asami, K., Sekine, K., 2007. J. Phys. D Appl. Phys. 40, 2197-2204.

Baron, T.H., Kamath, P.S., McBane, R.D., 2013. N. Engl. J. Med. 368, 2113–2124. Baughman, R.R., Lower, E.E., Flessa, H.C., Tollerud, D.J., 1993. Chest 104, 1243–1247.

Badginiani, A., Lower, E.E., Piessa, H.C., Tollerid, E.J., 1995. Clies 104, 1243–1247.
van Bladel, E.R., Roest, M., de Groot, P.G., Schutgens, R.E.G., 2011. Haematologica 96, 888–895.

Bolliger, D., Seeberger, M.D., Tanaka, K.A., 2012. Transfus. Med. Rev. 26, 1–13. Briggs, C., 2009. Int. J. Lab. Hematol. 31, 277–297.

Chakraverty, R., Davidson, S., Peggs, K., Stross, P., Garrard, C., Littlewood, T.J., 1996. Br. J. Haematol. 93, 460–463.

Chee, Y.-L., Greaves, M., 2003. Hematol. J. 4, 373-378.

Chelidze, T., 2002. J. Non-Cryst. Solids 305, 285-294.

Chen, A., Stecker, E., Warden, B.A., 2020. J. Am. Heart Assoc. 9, 17559.

Chiba, S., Uchibori, K., Fujiwara, T., Ogata, T., Yamauchi, S., Shirai, T., Masuo, M., Okamoto, T., Tateishi, T., Furusawa, H., Fujie, T., Sakashita, H., Tsuchiya, K., Tamaoka, M., Miyazaki, Y., Inase, N., Sumi, Y., 2015. J. Sci. Res. Reports 4, 180–188. Dahlbäck, B., 2000. Lancet 355, 1627–1632.

Dichiara, A.B., Song, A., Goodman, S.M., He, D., Bai, J., 2017. J. Mater. Chem. 5, 20161–20169.

Ganter, M.T., Hofer, C.K., 2008. Anesth. Analg. 106, 1366-1375.

Gillissen, A., Van Den Akker, T., Caram-Deelder, C., Henriquez, D.D.C.A., Bloemenkamp, K.W.M., De Maat, M.P.M., Van Roosmalen, J.J.M., Zwart, J.J., Eikenboom, J., Van Der Bom, J.G., 2018. Blood Adv. 2, 2433–2442.

Gissel, M., Brummel-Ziedins, K.E., Butenas, S., Pusateri, A.E., Mann, K.G., Orfeo, T., 2016. J. Thromb. Haemostasis 14, 2001–2010.

Gottumukkala, V.N.R., Sharma, S.K., Philip, J., Camenzind, V., Bombeli, T., Seifert, B., Jamnicki, M., Popovic, D., Pasch, T., Spahn, D.R., 1999. Anesth. Analg. 89, 1453–1455.

Green, D., McMahon, B., Foiles, N., Tian, L., 2008. Am. J. Clin. Pathol. 130, 811–815. Grünewald, M., Siegemund, A., Grünewald, A., Konegen, A., Koksch, M., Griesshammer, M., 2002. Platelets 13, 451–458.

Harris, L.F., Castro-López, V., Killard, A.J., 2013. TrAC Trends Anal. Chem. (Reference Ed.) 50, 85–95.

Harrison, P., 2009. Hämostaseologie 29, 25-31.

Hayashi, Y., Brun, M.A., Machida, K., Lee, S., Murata, A., Omori, S., Uchiyama, H., Inoue, Y., Kudo, T., Toyofuku, T., Nagasawa, M., Uchimura, I., Nakamura, T., Muneta, T., 2017. Biorheology 54, 25–35.

Hayashi, Y., Brun, M.A., Machida, K., Nagasawa, M., 2015. Anal. Chem. 87, 10072–10079.

Hayashi, Y., Katsumoto, Y., Omori, S., Yasuda, A., Asami, K., Kaibara, M., Uchimura, I., 2010. Anal. Chem. 82, 9769–9774.

Hayashi, Y., Oshige, I., Katsumoto, Y., Omori, S., Yasuda, A., Asami, K., 2008. Phys. Med. Biol. 53, 2553–2564.

Heileman, K., Daoud, J., Tabrizian, M., 2013. Biosens. Bioelectron. 49, 348–359.

Jackson, S.P., 2011. Nat. Med. 17, 1423–1436.

Jensen, M.S., Larsen, O.H., Christiansen, K., Fenger-Eriksen, C., Ingerslev, J., Sørensen, B., 2013. Haemophilia 19, 403–408.

Kahng, S.-J., Cerwyn, C., Dincau, B.M., Kim, J.-H., Novosselov, I.V., Anantram, M.P., Chung, J.-H., 2018. Nanotechnology 29, 335304.

Kattula, S., Byrnes, J.R., Wolberg, A.S., 2017. Fibrinogen and fibrin in hemostasis and thrombosis. Arterioscler. Thromb. Vasc. Biol. 37 (3), e13–e21.

Kirley, K., Qato, D.M., Kornfield, R., Stafford, R.S., Alexander, G.C., 2012. Circ. Cardiovasc. Qual. Outcomes 5, 615–621.

Levi, M., Opal, S.M., 2006. Crit. Care 10, 222.

Maji, D., De La Fuente, M., Kucukal, E., Sekhon, U.D.S., Schmaier, A.H., Sen Gupta, A., Gurkan, U.A., Nieman, M.T., Stavrou, E.X., Mohseni, P., Suster, M.A., 2018. J. Thromb. Haemostasis 16, 2050–2056.

Maji, D., Suster, M.A., Kucukal, E., Sekhon, U.D.S., Gupta, A. Sen, Gurkan, U.A., Stavrou, E.X., Mohseni, P., 2017. IEEE Trans. Biomed. Circuits Syst. 11, 1459–1469. Mallett, S.V., Armstrong, M., 2015. Anaesthesia 70, 73–77.

Mann, K., 1999. Thromb. Haemostasis 82, 165-174.

Marlar, R.A., Potts, R.M., Marlar, A.A., 2006. Am. J. Clin. Pathol. 126, 400-405.

Matchar, D.B., Samsa, G.P., Cohen, S.J., Oddone, E.Z., 2000. J. Thromb. Thrombolysis 9, S7–S11.

van der Meijden, P.E.J.J., Heemskerk, J.W.M.M., 2019. Nat. Rev. Cardiol. 16, 166–179. Michelson, A.D., 2019. Platelets, Platelets. Elsevier.

Di Minno, A., Frigerio, B., Spadarella, G., Ravani, A., Sansaro, D., Amato, M., Kitzmiller, J.P., Pepi, M., Tremoli, E., Baldassarre, D., 2017. Blood Rev. 31, 193–203. Nagler, M., Kathriner, S., Bachmann, L.M., Wuillemin, W.A., 2013. Thromb. Res. 131, 249–253.

- Ogawa, S., Szlam, F., Bolliger, D., Nishimura, T., Chen, E.P., Tanaka, K.A., 2012. Anesth. Analg. 115, 16–21.
- Pengo, V., Pegoraro, C., Cucchini, U., Iliceto, S., 2006. J. Thromb. Thrombolysis 21, 73–77.
- Penning-Van Beest, F.J.A., Van Meegen, E., Rosendaal, F.R., Stricker, B.H.C., 2001. Thromb. Haemostasis 86, 569–574.
- Pethig, R., 1984. IEEE Trans. Electr. Insul. 19, 453-474.
- Ranucci, M., Baryshnikova, E., 2020. J. Clin. Med. 9, 189.
- Rasmussen, K.C., Højskov, M., Johansson, P.I., Kridina, I., Kistorp, T., Salling, L., Nielsen, H.B., Ruhnau, B., Pedersen, T., Secher, N.H., 2016. Medicine (Baltim.) 95, e2720.
- Seiffge, D.J., De Marchis, G.M., Koga, M., Paciaroni, M., Wilson, D., Cappellari, M., Macha, M.D.K., Tsivgoulis, G., Ambler, G., Arihiro, S., Bonati, L.H., Bonetti, B., Kallmtinzer, B., Muir, K.W., Bovi, P., Gensicke, H., Inoue, M., Schwab, S., Yaghi, S., Brown, M.M., Lyrer, P., Takagi, M., Acciarrese, M., Jager, H.R., Polymeris, A.A., Toyoda, K., Venti, M., Traenka, C., Yamagami, H., Alberti, A., Yoshimura, S., Caso, V., Engelter, S.T., Werring, D.J., 2020. Ann. Neurol. 87, 677–687.
- Sørensen, B., Tang, M., Larsen, O.H., Laursen, P.N., Fenger-Eriksen, C., Rea, C.J., 2011. Thromb. Res. 128, S13–S16.

- Spiezia, L., Radu, C., Marchioro, P., Bertini, D., Rossetto, V., Castelli, M., Pagnan, A., Sørensen, B., Simioni, P., 2008. Thromb. Haemostasis 100, 1106–1110.
- Sullivan, P.W., Arant, T.W., Ellis, S.L., Ulrich, H., 2006. Pharmacoeconomics 24, 1021–1033.
- Tynngård, N., Lindahl, T.L., Ramström, S., 2015. Thromb. J. 13, 8.
- Ur, A., 1970. Nature 226, 269–270. Versteeg, H.H., Heemskerk, J.W.M., Levi, M., Reitsma, P.H., 2013. Physiol. Rev. 93,
- Versteeg, H.H., Heemskerk, J.W.M., Levi, M., Reitsma, P.H., 2013. Physiol. Rev. 93, 327–358.
- Wang, Y., Wang, M., Ni, Y., Liang, Z., 2020. Hematology 25, 63-70.
- Weisel, J.W., Litvinov, R.I., 2019. J. Thromb. Haemostasis 17, 271-282.
- Wells, P.S., Holbrook, A.M., Crowther, N.R., Hirsh, J., 1994. Ann. Intern. Med. 121, 676–683.
- Whiting, D., DiNardo, J.A., 2014. Am. J. Hematol. 89, 228-232.
- Zhang, J., Goodman, S.M., Wise, H.G., Dichiara, A.B., Chung, J.-H., 2021. J. Mater. Chem. C 9, 4544–4553.
- Zhu, J., Alexander, G.C., Nazarian, S., Segal, J.B., Wu, A.W., 2018. Pharmacotherapy 38, 907–920.